Weierstraß-Institut
für Angewandte Analysis und Stochastik
Leibniz-Institut im Forschungsverbund Berlin e. V.

Preprint ISSN 2198-5855

An assessment of two classes of variational multiscale methods for the simulation of incompressible turbulent flows

Naveed Ahmed[1], Volker John[2]

submitted: March 5, 2020

[1] Gulf University for Science and Technology
Department of Mathematics and Natural Sciences
Kuwait City, Kuwait
E-Mail: ahmed.n@gust.edu.kw

[2] Weierstrass Institute
Mohrenstr. 39, 10117 Berlin, Germany
and Freie Universität Berlin
Dep. of Mathematics and Computer Science
Arnimallee 6, 14195 Berlin, Germany
E-Mail: volker.john@wias-berlin.de

No. 2698
Berlin 2020

2010 *Mathematics Subject Classification.* 76F65.

Key words and phrases. Incompressible turbulent flows, residual-based VMS method, SUPG method, projection-based VMS method, turbulent channel flows, LSC preconditioner.

Edited by
Weierstraß-Institut für Angewandte Analysis und Stochastik (WIAS)
Leibniz-Institut im Forschungsverbund Berlin e. V.
Mohrenstraße 39
10117 Berlin
Germany

Fax: +49 30 20372-303
E-Mail: preprint@wias-berlin.de
World Wide Web: http://www.wias-berlin.de/

An assessment of two classes of variational multiscale methods for the simulation of incompressible turbulent flows

Naveed Ahmed, Volker John

Abstract

A numerical assessment of two classes of variational multiscale (VMS) methods for the simulation of incompressible flows is presented. Two types of residual-based VMS methods and two types of projection-based VMS methods are included in this assessment. The numerical simulations are performed at turbulent channel flow problems with various friction Reynolds numbers. It turns out the the residual-based VMS methods, in particular when used with a pair of inf-sup stable finite elements, give usually the most accurate results for second order statistics. For this pair of finite element spaces, a flexible GMRES method with a Least Squares Commutator (LSC) preconditioner proved to be an efficient solver.

1 Introduction

Let $\Omega \subset \mathbb{R}^3$ be a bounded domain with boundary Γ and $(0,T)$ be a bounded time interval. Incompressible flows are modeled by the incompressible Navier–Stokes equations (in dimensionless form): Find a velocity field $\boldsymbol{u} \ : \ (0,T] \times \Omega \ \rightarrow \ \mathbb{R}^3$ and a pressure field $p \ : \ (0,T] \times \Omega \rightarrow \mathbb{R}$ such that

$$\begin{aligned} \partial_t \boldsymbol{u} - 2\nu \nabla \cdot \mathbb{D}\left(\boldsymbol{u}\right) + (\boldsymbol{u} \cdot \nabla)\boldsymbol{u} + \nabla p &= \boldsymbol{f} \quad \text{in } (0,T] \times \Omega, \\ \nabla \cdot \boldsymbol{u} &= 0 \quad \text{in } (0,T] \times \Omega, \\ \boldsymbol{u}(0,\boldsymbol{x}) &= \boldsymbol{u}_0 \quad \text{in } \Omega, \end{aligned} \tag{1}$$

where $\mathbb{D}\left(\boldsymbol{u}\right) = \left(\nabla \boldsymbol{u} + (\nabla \boldsymbol{u}^T)\right)/2$ is the velocity deformation tensor, ν is the kinematic viscosity, $\boldsymbol{u}_0$ is a given initial velocity field, and $\boldsymbol{f}$ represents given body forces. System (1) has to be equipped with boundary conditions on Γ.

In particular, the behavior of turbulent incompressible flows is modeled with (1). There is no mathematical definition of what is a turbulent flow. A generally used characterization from the physical point of view is that turbulent flows possess a wide range of physically important scales, ranging from very large ones to very small ones. The smallest scales are important for the energy dissipation. From the point of view of numerical simulations, turbulent flows might be characterized as those whose range of important scales cannot be

DOI 10.20347/WIAS.PREPRINT.2698 Berlin 2020

resolved by the affordable fineness of the discrete model, where the fineness depends on the grid and, e.g., in the case of finite elements, on the polynomial degree. It turns out that in this situation, standard approaches like central finite differences or the Galerkin finite element method fail, i.e., the corresponding simulations usually blow up in finite time. These standard discretizations try to simulate the behavior of all important persistent scales. However, since usually most of the important persistent scales of turbulent flows cannot be represented by the affordable fineness of the discretization, these so-called unresolved scales cannot be simulated. The remedy consists in utilizing a so-called turbulence model, which should model the impact of the unresolved scales on the resolved scales. There are numerous proposals of turbulence models, see [26, 30] to mention just two standard references.

One class of turbulence models are Variational Multiscale (VMS) methods. VMS methods use a mathematical approach for defining a turbulence model, which might be enriched with a turbulence model based on physical insight into turbulent flows. The principal ideas of VMS methods were developed in [17, 16]. VMS methods are based on the variational or weak formulation of the underlying equation. A scale separation into resolved and unresolved scales is performed by projections into appropriate function spaces. Recent reviews of these models can be found in [2, 28]. For the sake of brevity, only a few important aspects, in particular from [2], will be mentioned here.

Several realizations of VMS methods can be found in the literature. One can distinguish between two-scale VMS methods, which just use a decomposition into resolved and unresolved scales, and three-scale VMS methods, where the resolved scales are decomposed once more in large resolved scales and small resolved scales. For all of these methods, one can find numerical studies in the literature, see the surveys presented in [2]. But there are only very few numerical comparisons of these methods among each other. The lack of such comparisons was mentioned as the main reason why it is not possible so far to provide a recommendation which VMS method(s) should be used in practice.

As already discussed in [2], we think that assessments of different numerical methods should be performed with the same code. In this way, a number of algorithmic choices, which might possess an unknown impact on the computational results, can be chosen to be the same for all methods, like the concrete finite element spaces, the explicit or implicit temporal treatment of certain terms, or the stopping criterion for the solver. All realizations of VMS methods go along with a considerable work for their implementation. Most probably, there are only few codes providing more than one VMS method. We think that this is a major reason why only a small number of papers with numerical comparisons of VMS methods is available. To be concrete, we are only aware of comparisons between the following classes of VMS methods. Two versions of a three-scale Algebraic VMS-Multigrid method were compared in [13, 14, 27] with the two-scale residual-based VMS method from [6]. In [20], a three-scale VMS method that is based on a projection of the velocity deformation tensor, from [18], is compared with a three-scale VMS method which uses bubble functions for scale separation. Recently, a comparison of the residual-based VMS method from [6], a simplification of this method, and two local projection stabilization (LPS) methods was presented in [3]. This comparison was

performed for a complex flow in two dimensions. However, it is well known that real turbulent flows possess important properties which cannot occur in two-dimensional flows, like vortex stretching.

The goal of the present paper consists in assessing approaches from two classes of VMS methods: two-scale residual-based VMS methods, originally proposed in [6], and three-scale projection-based VMS methods, proposed in [18]. In addition, a reduced version of the two-scale residual-based VMS method, a SUPG/PSPG/grad-div method (Streamline Upwind Petrov–Galerkin, pressure stabilized Petrov–Galerkin) is incorporated in the numerical studies. Besides the assessment of these two classes of VMS methods, there are some additional aspects that extend the available literature. For instance, besides utilizing equal order pairs of finite element spaces in the residual-based VMS methods, also an inf-sup stable pair is used. Firstly, both cases require different parameters in these methods and secondly, for inf-sup stable pairs, the unnecessary pressure-pressure coupling is neglected such that one obtains saddle point problems in contrast to the equal order pair. Another new aspect of this paper is the application of the eddy viscosity model proposed by Verstappen in [33] in the projection-based VMS method. In the literature, so far only the Smagorinsky model, which is also included in our studies, was applied.

The numerical studies are performed at standard benchmark problems for incompressible turbulent flow simulations, namely turbulent channel flows problems. In a preliminary study, a good value of one of the parameters of the residual-based VMS method, when using an inf-sup stable pair of finite element spaces, is determined. Another preliminary study investigates the choice of a parameter in the Verstappen eddy viscosity model. After having determined appropriate parameters, all methods are assessed at the turbulent channel flow problems. It turns out that the residual-based VMS methods often computed more accurate results, in particular with respect to second order quantities of interest. Concerning the efficiency of the simulations, a flexible GMRES method with a Least Squares Commutator (LSC) preconditioner proved to be an efficient approach in the case of the used inf-sup stable pair of finite element spaces.

The paper is organized as follows. Section 2 describes the studied VMS methods in some detail. The numerical results, first concerning the parameter studies mentioned above and then with respect to assess the VMS methods among each other, are presented in Section 3. A summary is provided in Section 4.

2 Variational Multiscale Methods

This section provides a brief description of the VMS methods that were involved in our computational studies. One can find detailed descriptions of these methods at several places in the literature, e.g., in [2].

Consider for simplicity of notation the case of homogeneous Dirichlet boundary conditions on $(0,T] \times \Gamma$. To define a variational formulation of the Navier–Stokes equations (1), the

velocity space $\boldsymbol{V} = [H_0^1(\Omega)]^3$ and the pressure space $Q = L_0^2(\Omega)$ are introduced. Let $(\cdot,\cdot)$ denote the $L^2(\Omega)$ inner product for scalar- and vector-valued functions with respect to Ω. Then, a variational formulation of (1) reads as follows: Find $(\boldsymbol{u}, p) \ : \ (0,T] \to \boldsymbol{V} \times Q$ such that for all $(\boldsymbol{v}, q) \in \boldsymbol{V} \times Q$

$$\begin{aligned} (\partial_t \boldsymbol{u}, \boldsymbol{v}) + 2\nu(\mathbb{D}(\boldsymbol{u}), \mathbb{D}(\boldsymbol{v})) + ((\boldsymbol{u}\cdot\nabla)\boldsymbol{u}, \boldsymbol{v}) - (\nabla\cdot\boldsymbol{v}, p) &= \langle \boldsymbol{f}, \boldsymbol{v}\rangle, \\ (\nabla\cdot\boldsymbol{u}, q) &= 0, \\ \boldsymbol{u}(0,\boldsymbol{x}) &= \boldsymbol{u}_0 \quad \text{in } \Omega. \end{aligned} \tag{2}$$

Here, $\langle\cdot,\cdot\rangle$ denotes the duality pairing between $\boldsymbol{V}$ and its dual $\boldsymbol{V}^* = [H^{-1}(\Omega)]^3$. The convective term will be denoted by

$$n(\boldsymbol{u}, \boldsymbol{v}, \boldsymbol{w}) = ((\boldsymbol{u}\cdot\nabla)\boldsymbol{v}, \boldsymbol{w}), \quad \boldsymbol{u}, \boldsymbol{v}, \boldsymbol{w} \in \boldsymbol{V}.$$

In our numerical studies, conforming spaces $\boldsymbol{V}^h \times Q^h$ are considered, i.e., $\boldsymbol{V}^h \subset \boldsymbol{V}$ and $Q^h \subset Q$.

As temporal discretization, the BDF2 (backward difference formula of order 2) method is applied. Denoted by $\boldsymbol{u}_n^h \in \boldsymbol{V}^h$ and $p_n^h \in Q^h$ approximations of the velocity and pressure fields at time instance t_n, then the approximation of the time derivative $\partial_t \boldsymbol{u}$ of the velocity field is defined by

$$D_t \boldsymbol{u}_{n+1}^h = \frac{1}{2\Delta t}\left(3\boldsymbol{u}_{n+1}^h - 4\boldsymbol{u}_n^h - \boldsymbol{u}_{n-1}^h\right), \quad n \geq 2.$$

In the first step, the backward Euler method was applied. To reduce the computational complexity associated with the considered VMS methods, a semi-implicit (IMEX) version of the BDF2 method was utilized. For this version, the convection field and the pressure were obtained by means of a linear extrapolation:

$$\widehat{\boldsymbol{u}}_{n+1}^h = 2\boldsymbol{u}_n^h - \boldsymbol{u}_{n-1}^h \quad \text{and} \quad \widehat{p}_{n+1}^h = 2p_n^h - p_{n-1}^h.$$

The BDF2 scheme is of second order and it is strongly A-stable. Its use facilitates in particular the application of the two-scale residual-based VMS and the SUPG method in comparison with the Crank–Nicolson scheme, which is also of second order, A-stable, but not strongly A-stable. This is because in the Crank–Nicolson scheme residuals at former time instances are needed, which is not the case for BDF2. Despite the favorable properties of BDF2, this method does not seem to be used widely in combinations with VMS methods. We are aware of [10] for applying it in combination with a residual-based VMS method and of the two-dimensional studies from [3].

2.1 Two-Scale Residual-Based (RB-)VMS Method

This two-scale VMS method was proposed in [6]. It has the form: Find $\boldsymbol{u}^h : (0,T] \to \boldsymbol{V}^h$, $p^h : (0,T] \to Q^h$ satisfying

$$\begin{aligned}
&\left(\partial_t \boldsymbol{u}^h, \boldsymbol{v}^h\right) + \left(2\nu\mathbb{D}\left(\boldsymbol{u}^h\right), \mathbb{D}\left(\boldsymbol{v}^h\right)\right) + n\left(\boldsymbol{u}^h, \boldsymbol{u}^h, \boldsymbol{v}^h\right) + \left(\nabla\cdot\boldsymbol{u}^h, q^h\right) \\
&\quad - \left(\nabla\cdot\boldsymbol{v}^h, p^h\right) - \kappa_{\mathrm{is}}\left(\mathbf{res}_{\mathrm{m}}^h, \nabla q^h\right) - \left(\mathrm{res}_{\mathrm{c}}^h, \nabla\cdot\boldsymbol{v}^h\right) + n\left(\mathbf{res}_{\mathrm{m}}^h, \boldsymbol{u}^h, \boldsymbol{v}^h\right) \\
&\quad + n\left(\boldsymbol{u}^h, \mathbf{res}_{\mathrm{m}}^h, \boldsymbol{v}^h\right) + n\left(\mathbf{res}_{\mathrm{m}}^h, \mathbf{res}_{\mathrm{m}}^h, \boldsymbol{v}^h\right) = \langle \boldsymbol{f}, \boldsymbol{v}^h\rangle
\end{aligned} \tag{3}$$

for all $\left(\boldsymbol{v}^h, q^h\right) \in \boldsymbol{V}^h \times Q^h$, with

$$\begin{pmatrix} \mathbf{res}_{\mathrm{m}}^h \\ \mathrm{res}_{\mathrm{c}}^h \end{pmatrix} = \begin{pmatrix} \boldsymbol{\tau}_{\mathrm{m}}\left(\boldsymbol{f} - \partial_t\boldsymbol{u}^h + \nu\Delta\boldsymbol{u}^h - \left(\boldsymbol{u}^h\cdot\nabla\right)\boldsymbol{u}^h - \nabla p^h\right) \\ -\tau_{\mathrm{c}}\left(\nabla\cdot\boldsymbol{u}^h\right) \end{pmatrix}. \tag{4}$$

The term $-\left(\mathrm{res}_{\mathrm{c}}^h, \nabla\cdot\boldsymbol{v}^h\right)$ is known as grad-div stabilization. In (4), $\boldsymbol{\tau}_{\mathrm{m}}$ is a vector-valued and τ_{c} is a scalar stabilization parameter. For pairs of finite element spaces that satisfy the discrete inf-sup condition, there is $\kappa_{\mathrm{is}} = 0$, else it is $\kappa_{\mathrm{is}} = 1$.

To the best of our knowledge, one can find in the literature only numerical studies with RB-VMS methods using so-called equal order spaces, i.e., the finite element spaces for velocity and pressure are of the same principal form, e.g., in [6, 11, 13, 10]. In this case, it is $\kappa_{\mathrm{is}} = 1$ and there is a pressure-pressure coupling via the term $-\left(\mathbf{res}_{\mathrm{m}}^h, \nabla q^h\right)$ such that the RB-VMS method (3) does not lead to a saddle point problem. However, the RB-VMS methodology can be applied of course also with inf-sup stable pairs of finite element spaces. In this case, a pressure-pressure coupling is not necessary for stabilization and it was not used in our simulations since $\kappa_{\mathrm{is}} = 0$ was set. In this way, one has to solve finally saddle point problems and tailored solvers for such problems can be utilized, see Section 3.5. In addition, this approach avoids the assembling of a block matrix and the performance of unnecessary matrix-vector multiplications. The numerical studies presented in this paper consider as well equal order as inf-sup stable pairs of finite element spaces.

The fully discrete linearized semi-implicit RB-VMS formulation of (3) reads: Find $\left(\boldsymbol{u}_{n+1}^h, p_{n+1}^h\right) \in \boldsymbol{V}^h \times Q^h$ such that

$$\begin{aligned}
&\left(D_t\boldsymbol{u}_{n+1}^h, \boldsymbol{v}^h\right) + \left(2\nu\mathbb{D}\left(\boldsymbol{u}_{n+1}^h\right), \mathbb{D}\left(\boldsymbol{v}^h\right)\right) + b\big(\widehat{\boldsymbol{u}}_{n+1}^h, \boldsymbol{u}_{n+1}^h, \boldsymbol{v}^h\big) + \left(\nabla\cdot\boldsymbol{u}_{n+1}^h, q^h\right) \\
&\qquad - \left(\nabla\cdot\boldsymbol{v}^h, p_{n+1}^h\right) - \kappa_{\mathrm{is}}\left(\mathbf{res}_{\mathrm{m},n+1}^h, \nabla q^h\right) - \left(\mathrm{res}_{\mathrm{c},n+1}^h, \nabla\cdot\boldsymbol{v}^h\right) \\
&\qquad + n\left(\mathbf{res}_{\mathrm{m},n+1}^h, \widehat{\boldsymbol{u}}_{n+1}^h, \boldsymbol{v}^h\right) + n\left(\widehat{\boldsymbol{u}}_{n+1}^h, \mathbf{res}_{\mathrm{m},n+1}^h, \boldsymbol{v}^h\right) \\
&\qquad + n\left(\mathbf{res}_{\mathrm{m},n+1}^h, \widehat{\mathbf{res}}_{\mathrm{m},n+1}^h, \boldsymbol{v}^h\right) = \langle \boldsymbol{f}_{n+1}, \boldsymbol{v}^h\rangle
\end{aligned} \tag{5}$$

for all $\left(\boldsymbol{v}^h, q^h\right) \in \boldsymbol{V}^h \times Q^h$, where the residuals are given by

$$\begin{aligned}
\mathbf{res}_{\mathrm{m},n+1}^h &= \boldsymbol{\tau}_{\mathrm{m}}\left(\boldsymbol{f}_{n+1} - D_t\boldsymbol{u}_{n+1}^h + \nu\Delta\boldsymbol{u}_{n+1}^h - \left(\widehat{\boldsymbol{u}}_{n+1}^h\cdot\nabla\right)\boldsymbol{u}_{n+1}^h - \nabla p_{n+1}^h\right), \\
\widehat{\mathbf{res}}_{\mathrm{m},n+1}^h &= \boldsymbol{\tau}_{\mathrm{m}}\left(\boldsymbol{f}_{n+1} - D_t\widehat{\boldsymbol{u}}_{n+1}^h + \nu\Delta\widehat{\boldsymbol{u}}_{n+1}^h - \left(\widehat{\boldsymbol{u}}_{n+1}^h\cdot\nabla\right)\widehat{\boldsymbol{u}}_{n+1}^h - \nabla\widehat{p}_{n+1}^h\right), \\
\mathrm{res}_{\mathrm{c},n+1}^h &= -\widehat{\tau}_{\mathrm{c}}\left(\nabla\cdot\boldsymbol{u}_{n+1}^h\right).
\end{aligned}$$

Thus, the fully discrete RB-VMS method combined with the semi-implicit BDF2 scheme requires only the solution of one linear problem at each time instance. As the notation suggests, the stabilization parameters $\boldsymbol{\tau}_{\mathrm{m}}$ and $\widehat{\tau}_{\mathrm{c}}$ do not depend on the concrete time instance.

As already mentioned, both equal-order and inf-sup stable pair of finite elements are used in the numerical studies. A crucial issue is the choice of the stabilization parameters in (5).

For equal order pairs of finite element spaces, the proposal given in [6, Eqs. (63)–(69)] was used. In this proposal, one needs the value of the constant c_{inv} of an inverse estimate, which is usually not known in practice. In [6], there is no concrete value given and we could not find such a value in the reference provided in this paper. However, c_{inv} is multiplied with the square of the viscosity, which is a very small factor for turbulent flows, such that the term with c_{inv} is most probably of minor importance. In fact, we performed simulations with $c_{\mathrm{inv}} \in \{1, 50, 100\}$ and could not observe substantial differences in the results. For brevity, these results are not presented in detail. All results presented below were computed with $c_{\mathrm{inv}} = 50$.

In the case of inf-sup stable pairs of finite element spaces, it is known from the Oseen equations that the stabilization parameters have to be chosen in a different way, e.g., see [23, Rem. 5.24]. The grad-div parameter $\widehat{\tau}_{\mathrm{c}}$ has to be chosen as a constant and the SUPG parameter in the form $\boldsymbol{\tau}_{\mathrm{m}} = \tau_{\mathrm{m}}\mathbb{I}$, where $\mathbb{I}$ is the identity matrix and $\tau_{\mathrm{m}} = \mathcal{O}(h_K^2)$, with h_K being a local width of the mesh cell K. Since anisotropic mesh cells are used in the numerical studies, there are several proposals for defining the local mesh width. Based on our experience, e.g., see [22] or [23, Ex. 8.128], we used for h_K the length of the shortest edge of K. All simulations were performed with $\tau_{\mathrm{m}} = 0.25\ h_K^2$. Note that because of the scaling with h_K^2, the SUPG parameter is usually of minor impact in the case of inf-sup stable pairs of finite element spaces. For choosing an appropriate grad-div parameter $\widehat{\tau}_{\mathrm{c}}$, preliminary numerical studies were performed that are presented in Section 3.2.

2.2 Reduced RB-VMS Method, SUPG Method

The term $n\left(\boldsymbol{u}^h, \mathbf{res}_{\mathrm{m}}^h, \boldsymbol{v}^h\right)$ and $n\left(\mathbf{res}_{\mathrm{m}}^h, \mathbf{res}_{\mathrm{m}}^h, \boldsymbol{v}^h\right)$ in (3) are computationally somewhat involved. Neglecting these terms leads to the traditional SUPG/PSPG/grad-div method (streamline upwind Petrov–Galerkin, pressure stabilization Petrov–Galerkin). This method will be denoted briefly by SUPG in the following. Of course, there is the question concerning the impact of the neglected terms in the results of numerical simulations. Recent studies of a two-dimensional flow at high Reynolds number in [3] do not show an advantage of using the RB-VMS method (3) instead of the SUPG method. To investigate this question also for turbulent flows, the SUPG method is included in the numerical studies presented in this paper.

The fully discrete SUPG method considered in the numerical studies is obtained by neglecting the last two terms on the left-hand side of (5).

2.3 Three-Scale Projection-Based (PB-)VMS Method

In this VMS method, proposed in [18] based on ideas from [24], a physically based turbulence model is applied to fluctuations of the velocity deformation tensor. To this end, a finite-dimensional space L^H of symmetric 3×3 tensor-valued functions is needed. Then, the fully implicit three-scale PB-VMS method discretized in time using the semi-implicit BDF2 method reads: Find $\left(\boldsymbol{u}_{n+1}^h, p_{n+1}^h, \mathbb{G}_{n+1}^H\right) \in \boldsymbol{V}^h \times Q^h \times L^H$ satisfying

$$\begin{aligned}
\left(D_t \boldsymbol{u}_{n+1}^h, \boldsymbol{v}^h\right) + \left(2\nu\mathbb{D}\left(\boldsymbol{u}_{n+1}^h\right), \mathbb{D}\left(\boldsymbol{v}^h\right)\right) + n(\widehat{\boldsymbol{u}}_{n+1}^h, \boldsymbol{u}_{n+1}^h, \boldsymbol{v}^h) \\
- \left(\nabla \cdot \boldsymbol{v}^h, p_{n+1}^h\right) + \left(\nu_{\mathrm{T},n+1}\left(\mathbb{D}\left(\boldsymbol{u}_{n+1}^h\right) - \mathbb{G}_{n+1}^H\right), \mathbb{D}\left(\boldsymbol{v}^h\right)\right) = \langle \boldsymbol{f}_{n+1}, \boldsymbol{v}^h \rangle \\
\left(\nabla \cdot \boldsymbol{u}_{n+1}^h, q^h\right) = 0, \\
\left(\mathbb{D}\left(\boldsymbol{u}_{n+1}^h\right) - \mathbb{G}_{n+1}^H, \mathbb{L}^H\right) = 0,
\end{aligned} \tag{6}$$

for all $\left(\boldsymbol{v}^h, q^h\right) \in \boldsymbol{V}^h \times Q^h$ and $\mathbb{L}^H \in L^H$. In (6), $\nu_{\mathrm{T},n+1}$ is a non-negative function that usually depends on the finite element velocity. Note that the fluctuations of the velocity deformation tensor are defined by a $L^2(\Omega)$ projection.

In the literature, so far only the Smagorinsky model [31]

$$\nu_{\mathrm{T},n+1} = C_S \delta^2 \|\mathbb{D}\left(\boldsymbol{u}_{n+1}^h\right)\|_{\mathrm{F}} \tag{7}$$

seemed to be used, where C_S is a user-chosen constant, δ is proportional to a local mesh width, and $\|\cdot\|_{\mathrm{F}}$ is the Frobenius norm of a tensor. The numerical simulations presented in Section 3 were performed with $\delta = 2h_K$, where h_K is the shortest edge of the mesh cell K. Numerical studies, e.g., in [22], showed that this measure of the filter width is more appropriate than, e.g., measures that depend on the cubic root of the volume of K. In a vicinity of the boundary, a van Driest damping [26, p. 599] of the following form is utilized

$$\nu_{\mathrm{T},n+1} = C_S \delta^2 \left(1 - \exp\left(-\frac{y^+}{26}\right)\right) \|\mathbb{D}\left(\boldsymbol{u}_{n+1}^h\right)\|_{\mathrm{F}}, \quad \text{if } y^+ < 5,$$

where y^+ is the viscous length scale. From previous numerical studies, it is known that good choices for the user-chosen constant are usually $C_S \in [0.01, 0.02]$, e.g., see [23, Ex. 8.277, 8.279, 8.280]. For brevity, only results obtained with $C_S = 0.015$ will be presented here.

The numerical studies presented in this paper use, besides the Smagorinsky model (7), also an eddy viscosity model proposed by Verstappen in [33]. Investigating the question when eddy viscosity damps subgrid scales sufficiently, a model was derived, whose simplest form is

$$\nu_{\mathrm{T},n+1} = 6\left(\frac{\delta_{\mathrm{Ver}}}{\pi}\right)^2 \frac{\left|\det\left(\mathbb{D}\left(\boldsymbol{u}_{n+1}^h\right)\right)\right|}{\|\mathbb{D}\left(\boldsymbol{u}_{n+1}^h\right)\|_{\mathrm{F}}^2}, \tag{8}$$

where δ_{Ver} is also here the user-chosen filter width. A study for determining an appropriate value of δ_{Ver} within the framework of the PB-VMS method is presented in Section 3.3. Note that at walls with no-slip boundary condition, the eddy viscosity model (8) vanishes, since

$\det\left(\mathbb{D}\left(\boldsymbol{u}_{n+1}^h\right)\right) = 0$ because the directional derivatives of the velocity in all tangential directions vanish.

One can find in the literature so far simulations with the PB-VMS method only in combination with a fully implicit Crank–Nicolson scheme. Note that, in contrast to the residual-based methods, using the Crank–Nicolson scheme does not increase the complexity of implementing the PB-VMS method.

The PB-VMS method (6) leads to a saddle point problem. Hence, the finite element velocity and pressure space need to satisfy the discrete inf-sup condition. In [18], it was shown that an efficient implementation of (6) is only possible if L^H consists of discontinuous functions. Possible choices that were used in the literature are piecewise constant (P_0) or piecewise linear (P_1^{disc}) tensors. An adaptive choice of the projection space was proposed in [21], however this approach is considerably more complicated to implement than the case of a fixed space L^H and it will not be considered in this paper. In our experience, e.g., see [23, Ex. 8.279, 8.280], results obtained with piecewise constant tensors were usually among the best results for this method. For brevity, only results with $L^H = (P_0)^{3\times 3}$ will be presented in Section 3. The corresponding method is denoted by PB-VMS0.

3 Numerical Studies

Numerical studies were performed at turbulent channel flow problems. These problems, defined in [25], are standard benchmark problems for assessing numerical methods for incompressible turbulent flow simulations.

3.1 Turbulent Channel Flows, Setup of the Simulations

Here, only a brief description of the examples are given because one can find such descriptions at many places in the literature. The description below follows [23, Ex. D.12].

Turbulent channel flows at three Reynolds numbers (based on the friction velocity) are considered: $\mathrm{Re}_\tau \in \{180, 395, 590\}$. The flow domain in the case $\mathrm{Re}_\tau = 180$ is given by

$$\Omega = (-2\pi, 2\pi) \times (0, 2) \times \left(-\frac{2}{3}\pi, \frac{2}{3}\pi\right)$$

and for the two higher Reynolds numbers, it is defined by

$$\Omega = (-\pi, \pi) \times (0, 2) \times \left(-\frac{\pi}{2}, \frac{\pi}{2}\right).$$

The body force in the Navier–Stokes equations is $\boldsymbol{f} = (1, 0, 0)^T$. In all cases, there are no-slip boundary conditions $\boldsymbol{u} = \boldsymbol{0}$ at the walls $y = 0$ and $y = 2$. In the other two directions, periodic boundary conditions are described. An initial velocity field is obtained by adding

some random noise to the known mean velocity profile from [25], see [15] or [23, Ex. D.12] for details.

Simulations were performed in the time interval $[0, 40]$. In the first ten time units, the flows were allowed to develop and statistics of the flow were computed in $[10, 40]$.

For discretizing the equations, finite element methods on hexahedral grids were utilized. Concretely, for the RB-VMS and the SUPG methods, the pairs Q_2/P_1^{disc} and Q_2/Q_2 were used. Here, Q_2 is the space of continuous piecewise polynomials, where in each term each factor might be a monomial up to degree two. The space P_1^{disc} consists of discontinuous functions that are piecewise linear. The pair Q_2/P_1^{disc} of finite element spaces is inf-sup stable whereas the pair Q_2/Q_2 is not. To the best of our knowledge, numerical simulations of the RB-VMS method with inf-sup stable finite elements cannot be found so far in the literature. In addition, simulations with the RB-VMS method using equal order spaces of higher order than first order are also rare in the literature. We are solely aware that in [6] second order NURBS were utilized for the RB-VMS method and P_2/P_2 elements in [10]. For the PB-VMS0 method, the inf-sup stable pair Q_2/P_1^{disc} was used and, as already mentioned, the projection space $L^H = (P_0)^{3\times 3}$. The use of higher order than Q_1 finite element spaces for the velocity is based on our experience that the computational results are generally considerably more accurate if Q_2 elements are used. Their implementation is not much more involved than those of Q_1 elements.

The hexahedral grids were of tensor product type. The mesh widths in stream-wise (x) and spanwise (z) direction were chosen to be equidistant. In normal direction (y), the meshes were refined towards the walls. There are several proposals in the literature on how to perform this refinement. From our own experience, e.g., see [19], choosing the nodes accordingly to

$$y_i = 1 - \cos\left(\frac{i\pi}{N_y}\right), \quad i = 0, \ldots, N_y,$$

where N_y is the number of mesh cells in wall normal direction, is an appropriate way. For different Reynolds numbers, grids with different fineness were utilized: a coarse grid for $\mathrm{Re}_\tau = 180$, a medium refined grid for $\mathrm{Re}_\tau \in \{395, 590\}$, and a fine grid for $\mathrm{Re}_\tau = 590$. Some data of the grids and the corresponding number of degrees of freedom are summarized in Table 1.

As already mentioned at the beginning of Section 2, BDF2 was used as temporal discretization. The length of the equidistant time step was set to be $\Delta t = 0.004$ for $\mathrm{Re}_\tau = 180$ and $\Delta t = 0.002$ for the other two Reynolds numbers.

For assessing the computational results, the standard reference mean profiles from [25] were used. As first order statistics, the mean velocity profile was considered, where the averaging is performed in space and time, denoted by $\langle\langle\cdot\rangle_s\rangle_t$. The difference to this profile is defined by

$$\boldsymbol{u}_{\mathrm{mean,sim}} - \boldsymbol{u}_{\mathrm{mean,ref}}. \tag{9}$$

Second order statistics that were monitored are one component of the Reynolds stress ten-

Table 1: Information on the used grids, where d.o.f. denotes the number of degrees of freedom. The space Q_2 includes always Dirichlet nodes.

	coarse	medium	fine
mesh cells	$8 \times 16 \times 8$	$16 \times 32 \times 16$	$32 \times 64 \times 32$
d.o.f. P_1^{disc}	4 096	32 768	262 144
d.o.f. Q_2 (scalar)	8 448	66 560	528 384
d.o.f. all Q_2/P_1^{disc}	29 440	232 448	1 847 296
d.o.f. all Q_2/Q_2	33 792	266 240	2 113 536

sor

$$\mathbb{T}^h_{12,\text{mean}} = \langle\langle u_1^h u_2^h\rangle_s\rangle_t - \langle\langle u_1^h\rangle_s\rangle_t\langle\langle u_2^h\rangle_s\rangle_t$$

and one rms (root mean squared) turbulence intensity

$$u^h_{1,\text{rms}} = \left| \mathbb{T}^h_{11,\text{mean}} - \frac{1}{3}\sum_{j=1}^{3} \mathbb{T}^h_{jj,\text{mean}} \right|^{1/2}.$$

The description of the solvers for the arising linear systems of equations is postponed to Section 3.5, where the computational costs of the methods will be discussed.

All simulations were performed with the code ParMooN [12, 34] at compute servers HP BL460c Gen9 2xXeon, Fourteen-Core 2600MHz, using 14 processors for the coarse and medium grid and 21 processors for the fine grid. The parallelization was performed on the basis of MPI.

3.2 Determining an Appropriate Value for τ_{c}^{n+1} in the RB-VMS and SUPG Method

All considered methods possess parameters that have to be chosen and their concrete choice might have a considerable impact on the computational results. The choices used in our simulations were already discussed to some extent at the end of Sections 2.1 and 2.3. An open issue from these discussions was an appropriate value for τ_{c} in the RB-VMS and SUPG methods for the case of using the inf-sup stable pair Q_2/P_1^{disc} of finite element spaces.

Preliminary computational studies were performed for determining an appropriate value for τ_{c} and results for the turbulent channel flow at $\text{Re}_\tau = 180$ obtained on the coarse grid are presented in Figures 1 and 2. Very similar results are obtained for the RB-VMS and the SUPG methods, such that for the sake of brevity, only results for the SUPG method are shown. From Figure 1, where a wider range for this parameter is considered, it can be seen that the best results are obtained for $\tau_{\text{c}} = 0.3$. Smaller values of this parameter lead to a less accurate curve for $\mathbb{T}^h_{12,\text{mean}}$ whereas larger values give also less accurate results with

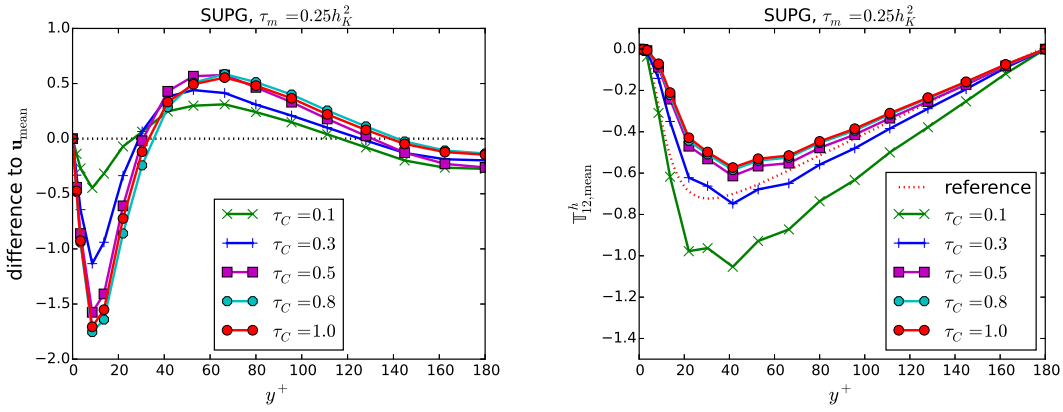

Figure 1: Turbulent channel flow at $\mathrm{Re}_\tau = 180$, coarse grid, SUPG method with Q_2/P_1^{disc}, results for different values of τ_c

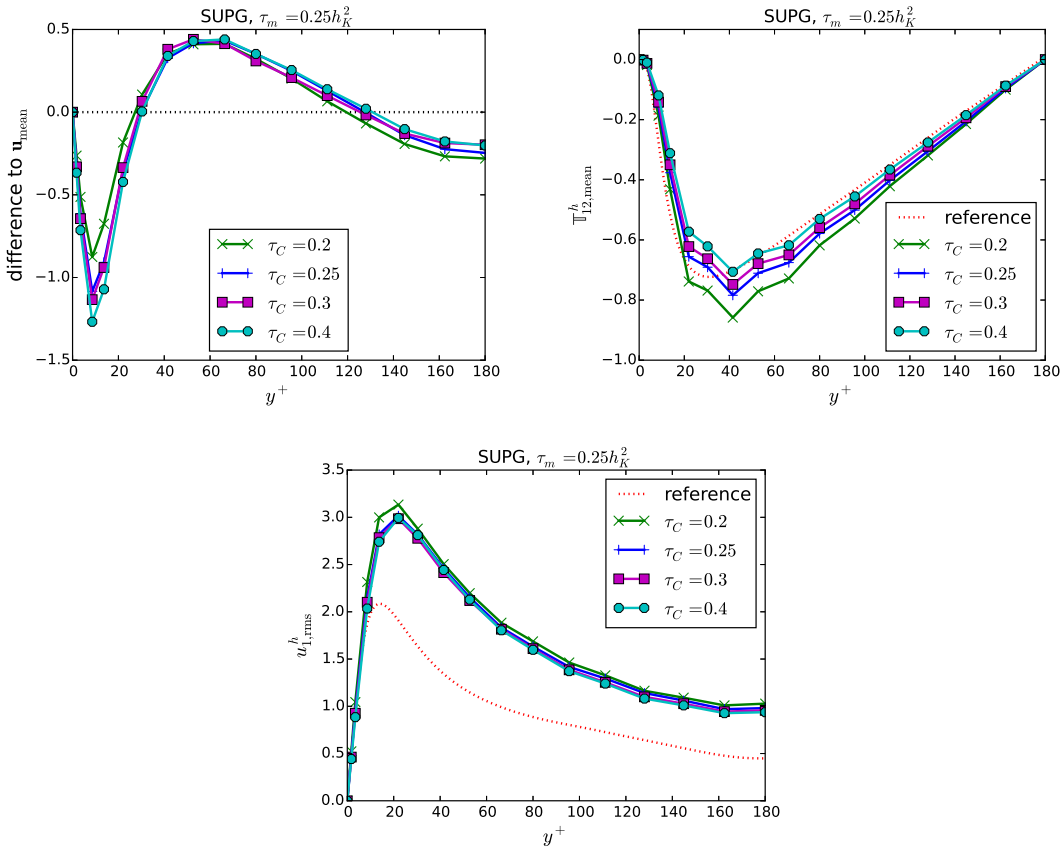

Figure 2: Turbulent channel flow at $\mathrm{Re}_\tau = 180$, coarse grid, SUPG method with Q_2/P_1^{disc}, results for different values of τ_c.

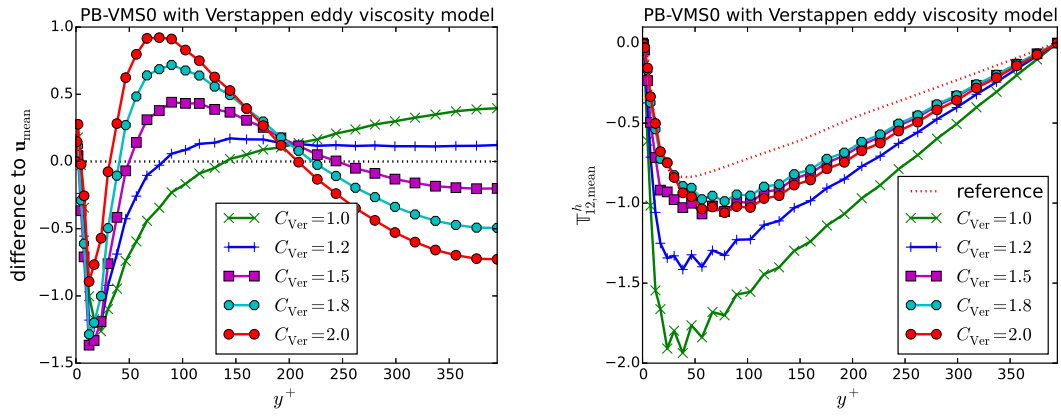

Figure 3: Turbulent channel flow at $\mathrm{Re}_\tau = 395$, medium grid, PB-VMS0 method with Verstappen eddy viscosity (8), different values of the filter width constant δ_{Ver}.

respect to the mean velocity profile. Having a closer look to this range of the parameter, see Figure 2, reveals that $\tau_{\text{c}} = 0.3$ is indeed an appropriate value. Altogether, we decided to use $\tau_{\text{c}} = 0.3$ for all subsequent simulations with the RB-VMS and the SUPG methods in combination with the Q_2/P_1^{disc} pair of finite element spaces.

3.3 Determining an Appropriate Value for δ_{Ver} in the Verstappen Eddy Viscosity Model (8)

As already explained at the end of Section 2.1, we chose as local mesh width h_K the length of the shortest edge of the mesh cell K. Then, the ansatz $\delta_{\text{Ver}} = C_{\text{Ver}} h_K$ was studied for the local filter width in the Verstappen eddy viscosity model (8).

Again, preliminary numerical studies were performed for determining an appropriate value for C_{Ver}. Results for the turbulent channel flow at $\mathrm{Re}_\tau = 395$ computed on the medium grid are presented in Figures 3 and 4. Figure 3 shows that better results are obtained with intermediate values of the considered set of values. Too large values lead to inaccurate mean velocity profiles and too small values to inaccurate results concerning $\mathbb{T}^h_{12,\text{mean}}$. More detailed studies presented in Figure 4 reveal that the best results are obtained with $C_{\text{Ver}} \in \{1.5, 1.6\}$. Among these values, the error in the mean velocity is somewhat smaller for $C_{\text{Ver}} = 1.5$ and the result for $\mathbb{T}^h_{12,\text{mean}}$ is a little bit better for $C_{\text{Ver}} = 1.6$. The results for $u^h_{1,\text{rms}}$, not shown here for brevity, are almost identical for both values. We decided to use $C_{\text{Ver}} = 1.5$ in all other simulations of the PB-VMS method with the Verstappen eddy viscosity model presented in this paper.

Comparing the final scaling that was used in our simulations with the somewhat more complicated approach utilized in [33], one finds that the scaling in our simulations is a little bit smaller. For example, close to the walls, for anisotropic mesh cells, the scaling is approxi-

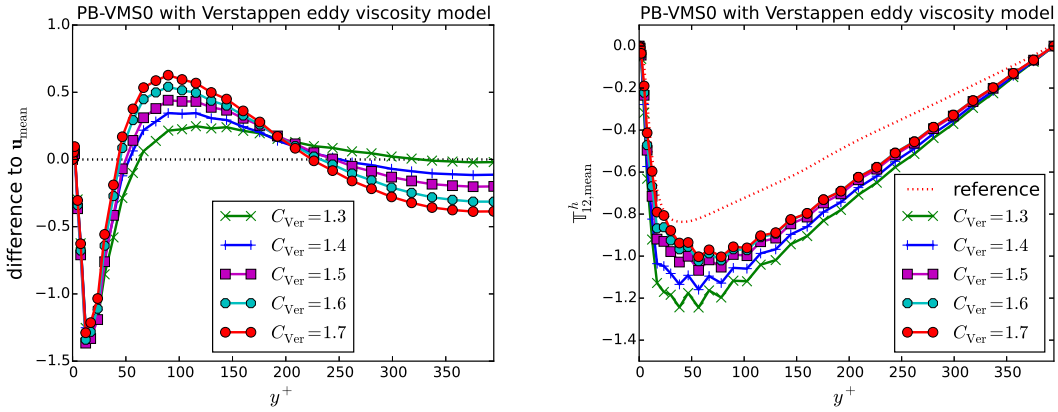

Figure 4: Turbulent channel flow at $\mathrm{Re}_\tau = 395$, medium grid, PB-VMS0 method with Verstappen eddy viscosity (8), different values of the filter width constant δ_{Ver}.

mately $1.5h_K^2$ in [33] and $1.37h_K^2$ here, where in both cases h_K is again the length of the shortest edge of K. Note that in [33], the proposed eddy viscosity model was used as a LES model and not within a VMS method.

3.4 Assessment of the VMS Methods with Respect to the Reference Profiles

The computational results with respect to the reference profiles for the turbulent channel flows at $\mathrm{Re}_\tau \in \{180, 395, 590\}$ are presented in Figures 5–8. The choice of the parameters for the individual methods is given in Sections 2.1, 2.3, 3.2, and 3.3.

Turbulent channel flow at $\mathrm{Re}_\tau = 180$. The results for this case are presented in Figure 5. Concerning the mean velocity profile, one can see that there are notable differences between the RB-VMS and SUPG methods, on the one hand, and the PB-VMS0 methods, on the other hand, in particular close to the wall. Whereas the former methods predict a mean velocity that is too small, since there is a negative value of (9), the latter methods give an over-prediction. For the RB-VMS and the SUPG methods, the results with the Q_2/P_1^{disc} pair are somewhat more accurate than with the Q_2/Q_2 pair. Considering the PB-VMS0 methods, better results are obtained with the Verstappen model in comparison with the Smagorinsky model.

The profile for $\mathbb{T}^h_{12,\mathrm{mean}}$ was predicted more accurately with the RB-VMS and SUPG methods than with the PB-VMS0 methods. Again, within these classes of methods, the Q_2/P_1^{disc} behaves better for the former classes, in particular for the SUPG method, and the Verstappen model for the latter class.

With respect to $u^h_{1,\mathrm{rms}}$, there are only minor differences between all obtained results. The best one is computed with the PB-VMS0 method using the Verstappen model. Here, the use of Q_2/Q_2 leads to a little bit better results for the RB-VMS and SUPG methods than the use

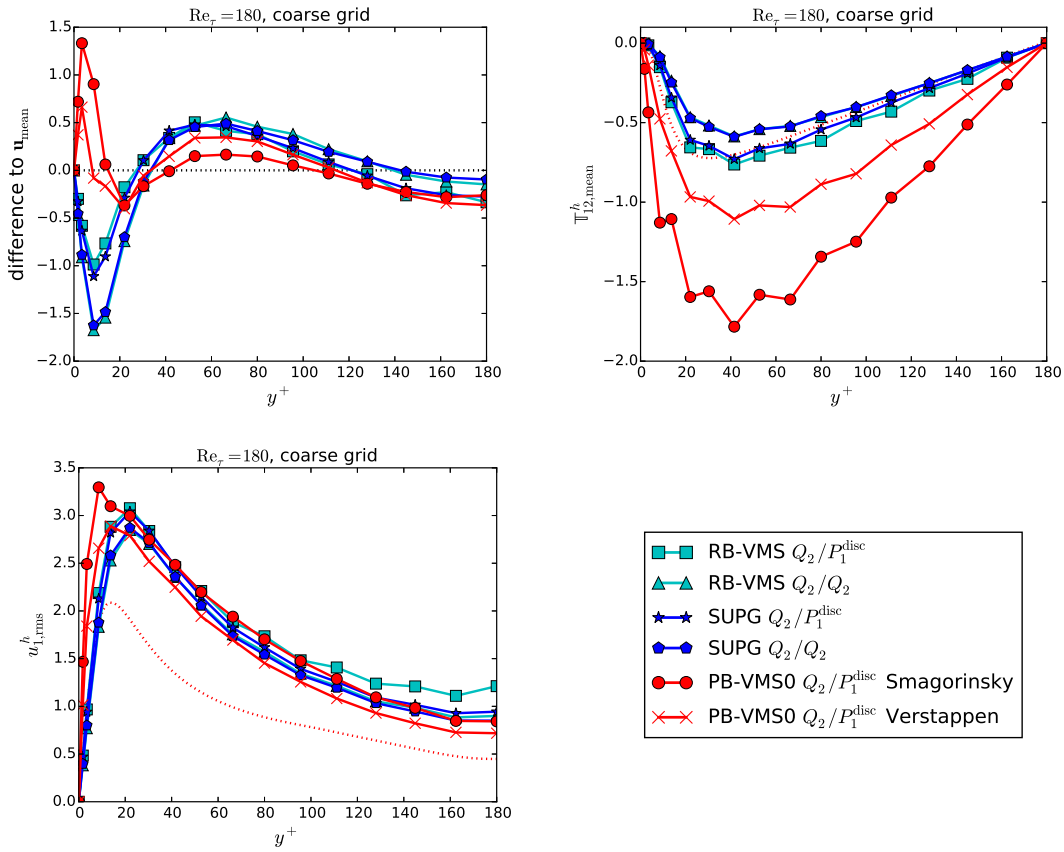

Figure 5: Turbulent channel flow at $\mathrm{Re}_\tau = 180$, coarse grid. Comparisons with reference profiles.

of the Q_2/P_1^{disc} pair of spaces.

In summary, the different classes of VMS methods give different results, in particular with respect to the mean velocity profile close to the boundary and the profile of $\mathbb{T}^h_{12,\mathrm{mean}}$. The RB-VMS and SUPG methods are considerably more accurate for $\mathbb{T}^h_{12,\mathrm{mean}}$ For these methods, somewhat better results are obtained with the Q_2/P_1^{disc} pair of finite element spaces. There are usually only negligible differences between the results computed with RB-VMS and SUPG if the same pair of finite element spaces is used. Concerning the PB-VMS0 methods, the use of the Verstappen model leads to more accurate results than the application of the Smagorinsky model.

Turbulent channel flow at $\mathrm{Re}_\tau = 395$. Computational results obtained for this example are displayed in Figure 6. Their evaluation reveals a few differences in comparison to the flow at $\mathrm{Re}_\tau = 180$.

The PB-VMS0 method with the Verstappen model under-predicts the mean velocity close to the boundary. Concerning this reference profile, the PB-VMS0 methods computed better

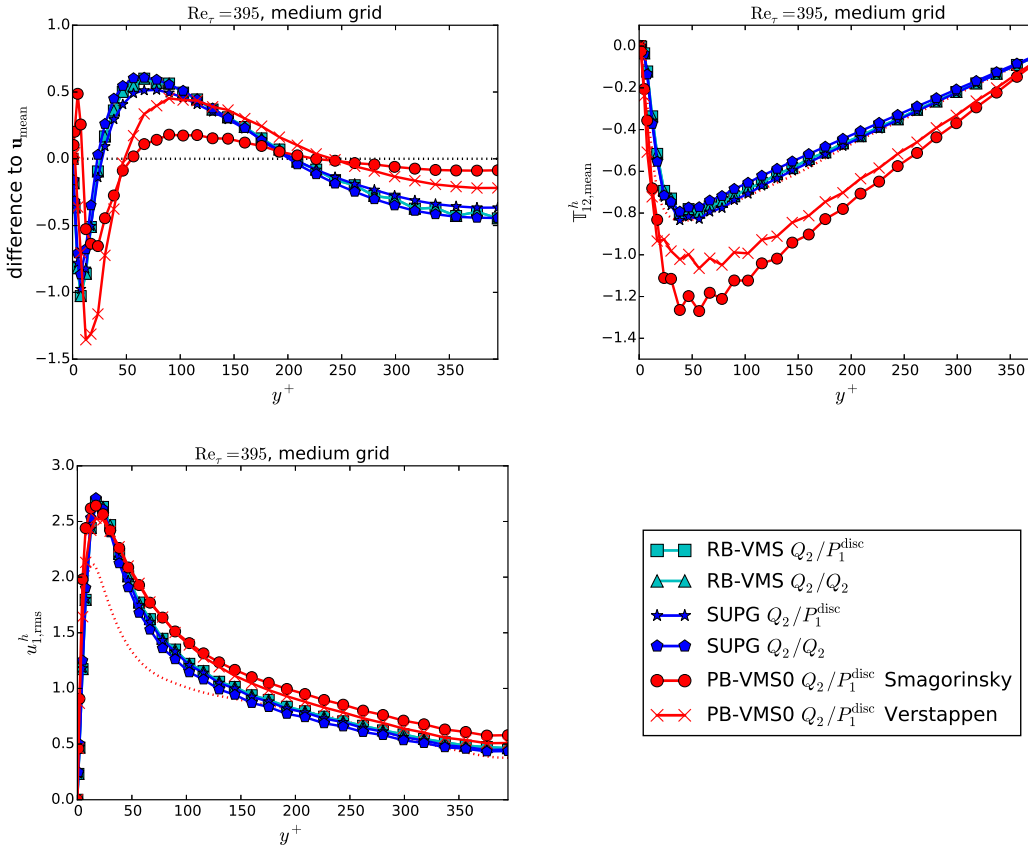

Figure 6: Turbulent channel flow at $\mathrm{Re}_\tau = 395$, medium grid. Comparisons with reference profiles.

results in the center of the channel. Among these methods, the Smagorinsky model gives the more accurate velocity profile. However, with respect to $\mathbb{T}^h_{12,\mathrm{mean}}$ and $u^h_{1,\mathrm{rms}}$, the profiles obtained with the Verstappen model are somewhat closer to the reference profiles.

Like in the $\mathrm{Re}_\tau = 180$ case, the RB-VMS and SUPG methods lead to considerably better results for $\mathbb{T}^h_{12,\mathrm{mean}}$, compared with the PB-VMS0 methods. Also the profiles for $u^h_{1,\mathrm{rms}}$ are a little bit more accurate. For the SUPG methods, the results with respect to the mean velocity and $\mathbb{T}^h_{12,\mathrm{mean}}$ are slightly more accurate if the Q_2/P_1^{disc} pair of spaces was used, instead of the Q_2/Q_2 pair.

Summarizing, the most striking difference of the results computed with the various VMS methods is the different accuracy with respect to $\mathbb{T}^h_{12,\mathrm{mean}}$. Again, the RB-VMS and SUPG methods lead to notably more accurate results. All results computed with the RB-VMS and SUPG methods are rather similar. For the PB-VMS0 methods, the second order quantities of interest are predicted somewhat more accurately if the Verstappen model was used.

Turbulent channel flow at $\mathrm{Re}_\tau = 590$. Computational studies for this case were performed

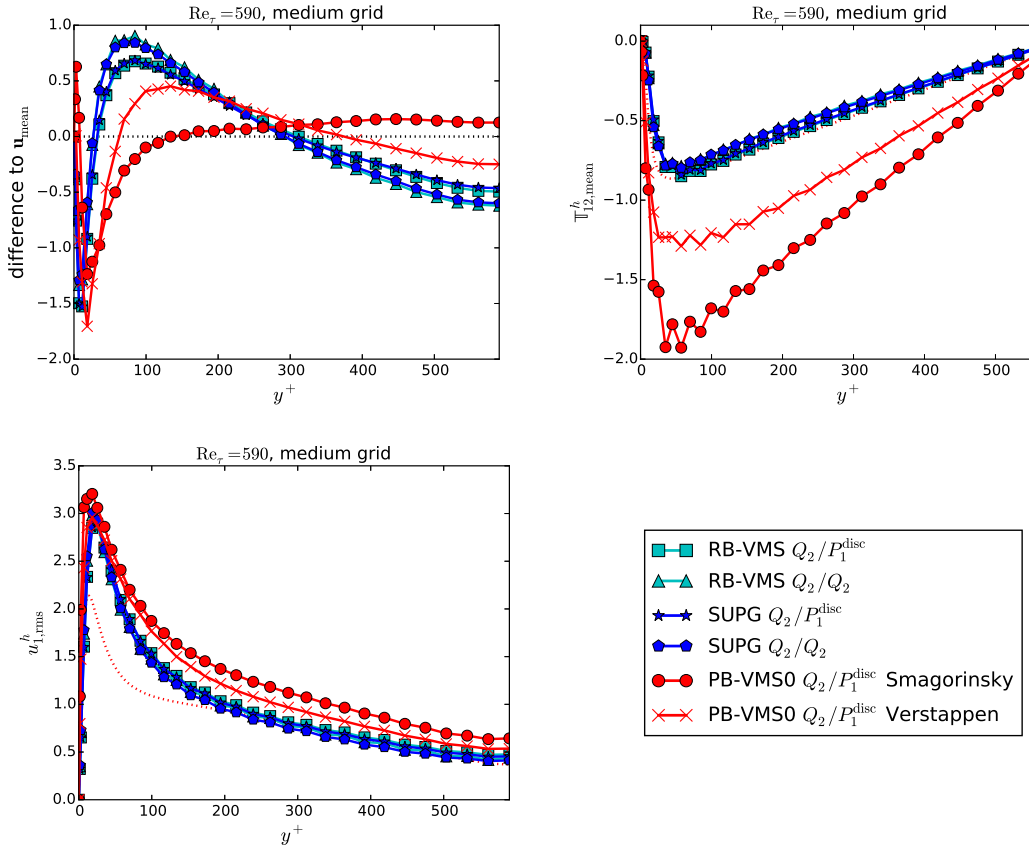

Figure 7: Turbulent channel flow at $\mathrm{Re}_\tau = 590$, medium grid. Comparisons with reference profiles. Note that the curves for the SUPG methods are often on top of the corresponding curves for the RB-VMS methods.

on the medium and the fine grid, see Figures 7 and 8 for the corresponding results. On the medium grid, the PB-VMS0 methods predict a more accurate mean velocity in the center of the channel, in particular the PB-VMS0 method with Smagorinsky model. On the fine grid, however, the results of the PB-VMS0 methods are not longer more accurately for the mean velocity and among these methods, the Verstappen model gives a somewhat better result. Concerning both second order quantities of interest, the RB-VMS and SUPG results are clearly more accurate than the results obtained with the PB-VMS0 methods. There are almost no visible differences between the curves of the RB-VMS and the SUPG method for the same pair of finite element spaces. On the medium grid, the results for $\mathbb{T}^h_{12,\mathrm{mean}}$ computed with the pair Q_2/P_1^{disc} are slightly better than those computed with the pair Q_2/Q_2. For all other second order quantities of interest, the curves for both pairs of finite element spaces are almost on top of each other.

In summary, the most notable observation for turbulent channel flow at $\mathrm{Re}_\tau = 590$ is that the predictions of the second order quantities of interest are computed much more accurately

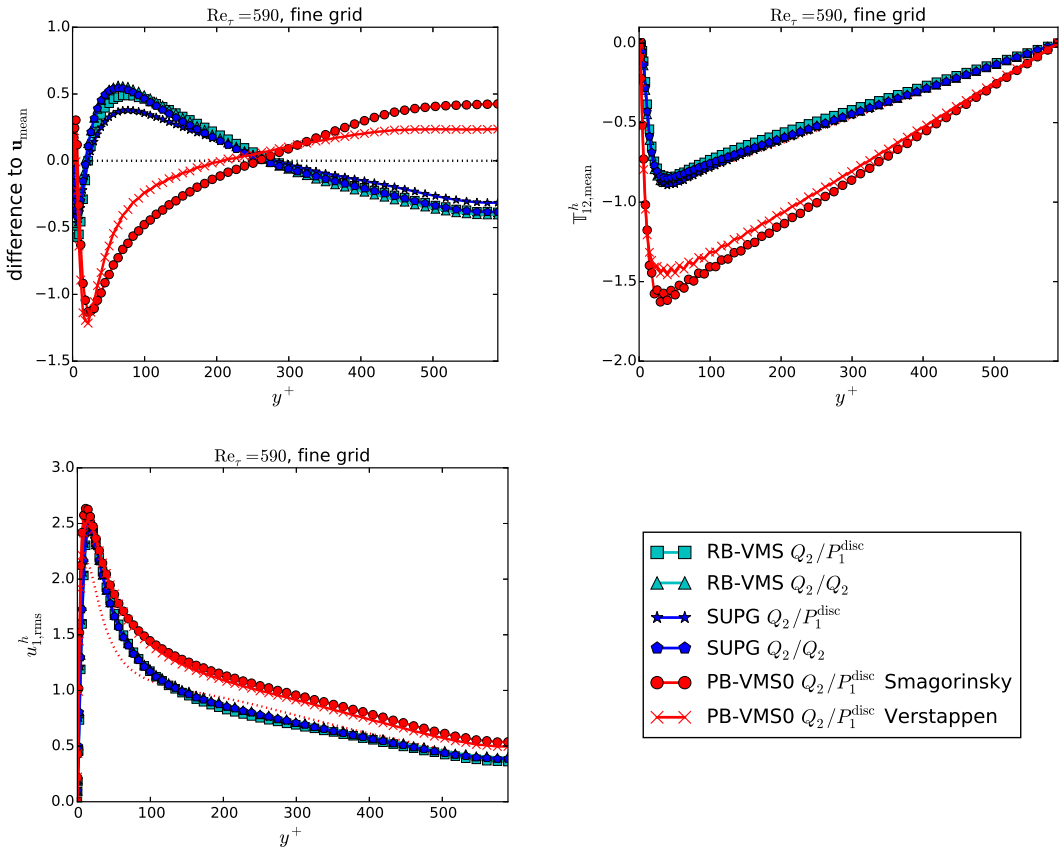

Figure 8: Turbulent channel flow at $\mathrm{Re}_\tau = 590$, fine grid. Comparisons with reference profiles. Note that the curves for the SUPG methods are often on top of the corresponding curves for the RB-VMS methods.

for the RB-VMS and SUPG methods compared with the PB-VMS0 methods.

3.5 Computational Costs

The main goal of our numerical studies was the assessment of the VMS methods with respect to the accuracy of the results and a comprehensive comparison of them with respect to efficiency is beyond the scope of the paper. But of course, we tried to perform efficient simulations utilizing the methods that were provided by the used code.

As already mentioned, the simulations were performed with a MPI parallelized code using 14 processors for the coarse and medium grid and 21 processors for the fine grid.

By construction, a computational overhead of all methods consists in assembling additional terms compared with the Galerkin finite element discretization of the Navier–Stokes equations. For the RB-VMS and the SUPG methods, these residual-based terms are calculated

by local computations. For the PB-VMS0 methods, an assembling of some matrices connected with the space L^H is necessary at the initial time and then the assembling of the additional terms in each discrete time requires few matrix-vector products with these matrices, see [18] or [23, Rem. 8.275] for details. Thus, the computational overhead for all methods is comparable from the point of view of assembling.

The arising linear systems of equations were solved iteratively, with the flexible GMRES method [29] as iterative solver. For efficient simulations, this method has to be equipped with an appropriate preconditioner. The stopping criterion for the flexible GMRES method was that the Euclidean norm of the residual vector was below $7 \cdot 10^{-7}$.

Using the inf-sup stable pair of finite element spaces $Q_2/P_1^{\rm disc}$ leads in all considered VMS methods to a linear saddle point problem to be solved in each time instance of the IMEX method. A study of solvers for linear saddle point problems was presented recently in [1]. This study considered laminar flows, the Galerkin finite element method, and serial simulations. For time-dependent problems, it was demonstrated in [1] that the so-called Least Squares Commutator (LSC) preconditioner from [7, 9] works efficiently. In particular, the efficiency of this preconditioner benefits from small time steps. For the simulations presented here, we used the same preconditioner, but now for turbulent flows, the VMS methods, and parallel simulations. For brevity, only the most important components of this preconditioner will be described, for a detailed description, we refer to the original sources [7, 9]. In the LSC preconditioner, one has to solve in each preconditioning step two systems for the pressure, where the matrix can be interpreted as a discretization of a scaled Poisson equation, and one system for the velocity. The matrix for the pressure system is the same for all time instances. The same strategy as in [1] was used, i.e., this matrix was explicitely computed, factorized with a parallel sparse solver, concretely with MUMPS [4, 5], and afterwards the triangular systems with the factors were solved. Note that the expensive steps, the explicit computation and the factorization of the matrix, have to be performed only in the first time step. The velocity system was solved iteratively with BiCGStab [32] and the SSOR preconditioner with relaxation parameter $\omega = 1$. A so-called inexact solve was performed, stopping the BiCGStab iteration after having reduced the Euclidean norm of the residual by the factor 10^4.

Utilizing the equal order pair Q_2/Q_2 introduces a pressure-pressure block in the linear system of equations due to the stabilization with respect to the violation of the discrete inf-sup condition. The LSC preconditioner can be extended to stabilized discretizations with first order velocity and pressure finite element spaces, see [8]. We are not aware of an extension to equal order pairs of finite element spaces of higher order. For this reason, the other type of preconditioner that was studied in [1] was utilized, namely a geometric multigrid method. The multiple discretization type of this method and a Vanka smoother were used. The Vanka smoother is a block Gauss–Seidel method. The multigrid F-cycle was applied with three pre and three post smoothing steps. For details concerning this preconditioner, we refer to [23, Chapter 9.2.2] and [1].

Information with respect to the computing times and the number of flexible GMRES iterations

Table 2: Efficiency of the VMS methods. First row for each method: computing time for the interval $[0, 40]$ in seconds, rounded to three leading digits; second row for each method: average number of flexible GMRES iterations per time step, rounded to the first digit after the comma. Note that 10 000 time steps were performed for $\mathrm{Re}_\tau = 180$ and 20 000 time steps for the other Reynolds numbers.

	$\mathrm{Re}_\tau = 180$ coarse	$\mathrm{Re}_\tau = 395$ medium	$\mathrm{Re}_\tau = 590$ medium	$\mathrm{Re}_\tau = 590$ fine
RB-VMS	1.61e4	1.65e5	2.10e5	1.31e6
Q_2/P_1^{disc}	7.6	6.4	10.9	5.5
RB-VMS	2.02e5	1.49e6	1.51e6	6.84e6
Q_2/Q_2	3.2	2.9	3.0	3.6
SUPG	2.09e4	2.06e5	2.17e5	3.82e6
Q_2/P_1^{disc}	9.5	10.2	10.9	19.5
SUPG	2.01e5	1.24e6	1.26e6	5.58e6
Q_2/Q_2	3.2	2.9	3.0	2.9
PB-VMS0	1.02e4	8.19e4	7.85e4	8.05e5
Smagorinsky	7.7	5.8	5.9	6.8
PB-VMS0	9.70e3	8.59e4	8.97e4	7.65e5
Verstappen	7.4	5.8	5.9	6.8

are provided in Table 2. It should be noted that the individual LSC steps might take different times since there is usually a different number of BiCGStab iterations for the velocity system. The most efficient simulations were performed with the PB-VMS0 method. Obviously, the LSC preconditioner works well. Only a slight dependency of the number of flexible GMRES iterations on the Reynolds number can be observed. For the RB-VMS and SUPG methods with the Q_2/P_1^{disc} pair of finite element spaces, flexible GMRES with LSC needed usually more iterations (with one exception) and always more time than for PB-VMS0. In three situations, the simulations were considerably more efficient for the RB-VMS method, compared with the SUPG method. Thus, the additional terms of the RB-VMS method seemed to possess a positive impact on the efficiency of the LSC preconditioner. In the equal order case, the multigrid preconditioner worked very well concerning the number of flexible GMRES iterations, but quite inefficiently with respect to computing times. One preconditioning step is simply too expensive. As already observed in [1], this preconditioner does not take advantage from small time steps. Finding and implementing a more efficient solver will be future work.

4 Summary

The most important conclusions from the numerical studies are as follows:

- Taking the results for all quantities of interest into account, the RB-VMS and SUPG methods gave more accurate results than the PB-VMS0 methods. This observation holds true in particular for the second order statistics, and there in particular for the Reynolds stress tensor $\mathbb{T}^h_{12,\mathrm{mean}}$.

- There were usually only little differences between the results obtained with the RB-VMS methods and the SUPG methods.

- The results computed with the inf-sup stable pair Q_2/P_1^{disc} of finite element spaces within the RB-VMS and the SUPG methods were often slightly more accurate than the result computed with the equal order finite element pair Q_2/Q_2 and the same methods.

- Concerning the PB-VMS0 methods, the Verstappen eddy viscosity model gave often more accurate results than the Smagorinsky eddy viscosity model.

- The LSC preconditioner worked usually efficiently for the methods with the inf-sup stable pair Q_2/P_1^{disc}. It needed less computing time for the PB-VMS methods than for the RB-VMS and the SUPG methods. The additional terms of the RB-VMS method, in comparison with the SUPG method, seemed to have a positive impact on the efficiency of the LSC preconditioner.

On the basis of our studies, the RB-VMS method with the Q_2/P_1^{disc} pair of finite element spaces can be recommended. The results with the SUPG method and the same pair of spaces were almost identical, but the simulations were less efficient.

References

References

[1] Naveed Ahmed, Clemens Bartsch, Volker John, and Ulrich Wilbrandt. An assessment of some solvers for saddle point problems emerging from the incompressible Navier-Stokes equations. *Comput. Methods Appl. Mech. Engrg.*, 331:492–513, 2018.

[2] Naveed Ahmed, Tomás Chacón Rebollo, Volker John, and Samuele Rubino. A review of variational multiscale methods for the simulation of turbulent incompressible flows. *Arch. Comput. Methods Eng.*, 24(1):115–164, 2017.

[3] Naveed Ahmed and Samuele Rubino. Numerical comparisons of finite element stabilized methods for a 2d vortex dynamics simulation at high reynolds number. *Computer Methods in Applied Mechanics and Engineering*, 349:191 – 212, 2019.

[4] Patrick R. Amestoy, Iain S. Duff, Jean-Yves L'Excellent, and Jacko Koster. A fully asynchronous multifrontal solver using distributed dynamic scheduling. *SIAM J. Matrix Anal. Appl.*, 23(1):15–41 (electronic), 2001.

[5] Patrick R. Amestoy, Abdou Guermouche, Jean-Yves L'Excellent, and Stéphane Pralet. Hybrid scheduling for the parallel solution of linear systems. *Parallel Comput.*, 32(2):136–156, 2006.

[6] Y. Bazilevs, V. M. Calo, J. A. Cottrell, T. J. R. Hughes, A. Reali, and G. Scovazzi. Variational multiscale residual-based turbulence modeling for large eddy simulation of incompressible flows. *Comput. Methods Appl. Mech. Engrg.*, 197(1-4):173–201, 2007.

[7] Howard Elman, Victoria E. Howle, John Shadid, Robert Shuttleworth, and Ray Tuminaro. Block preconditioners based on approximate commutators. *SIAM J. Sci. Comput.*, 27(5):1651–1668, 2006.

[8] Howard Elman, Victoria E. Howle, John Shadid, David Silvester, and Ray Tuminaro. Least squares preconditioners for stabilized discretizations of the Navier-Stokes equations. *SIAM J. Sci. Comput.*, 30(1):290–311, 2008.

[9] Howard C. Elman, David J. Silvester, and Andrew J. Wathen. *Finite elements and fast iterative solvers: with applications in incompressible fluid dynamics*. Numerical Mathematics and Scientific Computation. Oxford University Press, Oxford, second edition, 2014.

[10] Davide Forti and Luca Dedè. Semi-implicit BDF time discretization of the Navier-Stokes equations with VMS-LES modeling in a high performance computing framework. *Comput. & Fluids*, 117:168–182, 2015.

[11] P. Gamnitzer, V. Gravemeier, and W. A. Wall. Time-dependent subgrid scales in residual-based large eddy simulation of turbulent channel flow. *Comput. Methods Appl. Mech. Engrg.*, 199(13-16):819–827, 2010.

[12] S. Ganesan, V. John, G. Matthies, R. Meesala, S. Abdus, and U. Wilbrandt. An object oriented parallel finite element scheme for computing pdes: Design and implementation. In *IEEE 23rd International Conference on High Performance Computing Workshops (HiPCW) Hyderabad*, pages 106–115. IEEE, 2016.

[13] V. Gravemeier, M. W. Gee, M. Kronbichler, and W. A. Wall. An algebraic variational multiscale-multigrid method for large eddy simulation of turbulent flow. *Comput. Methods Appl. Mech. Engrg.*, 199(13-16):853–864, 2010.

[14] V. Gravemeier, M. Kronbichler, M. W. Gee, and W. A. Wall. An algebraic variational multiscale-multigrid method for large-eddy simulation: generalized-α time integration, Fourier analysis and application to turbulent flow past a square-section cylinder. *Comput. Mech.*, 47(2):217–233, 2011.

[15] Volker Gravemeier. Scale-separating operators for variational multiscale large eddy simulation of turbulent flows. *J. Comput. Phys.*, 212(2):400–435, 2006.

[16] J.-L. Guermond. Stabilization of Galerkin approximations of transport equations by subgrid modeling. *M2AN Math. Model. Numer. Anal.*, 33(6):1293–1316, 1999.

[17] T. J. R. Hughes. Multiscale phenomena: Green's functions, the Dirichlet-to-Neumann formulation, subgrid scale models, bubbles and the origins of stabilized methods. *Comput. Methods Appl. Mech. Engrg.*, 127(1-4):387–401, 1995.

[18] V. John and S. Kaya. A finite element variational multiscale method for the Navier-Stokes equations. *SIAM J. Sci. Comput.*, 26(5):1485–1503 (electronic), 2005.

[19] V. John and A. Kindl. Variants of projection-based finite element variational multiscale methods for the simulation of turbulent flows. *Internat. J. Numer. Methods Fluids*, 56(8):1321–1328, 2008.

[20] V. John and A. Kindl. Numerical studies of finite element variational multiscale methods for turbulent flow simulations. *Comput. Methods Appl. Mech. Engrg.*, 199(13-16):841–852, 2010.

[21] V. John and A. Kindl. A variational multiscale method for turbulent flow simulation with adaptive large scale space. *J. Comput. Phys.*, 229(2):301–312, 2010.

[22] V. John and M. Roland. Simulations of the turbulent channel flow at $\mathrm{Re}_\tau = 180$ with projection-based finite element variational multiscale methods. *Internat. J. Numer. Methods Fluids*, 55(5):407–429, 2007.

[23] Volker John. *Finite element methods for incompressible flow problems*, volume 51 of *Springer Series in Computational Mathematics*. Springer, Cham, 2016.

[24] W. Layton. A connection between subgrid scale eddy viscosity and mixed methods. *Appl. Math. Comput.*, 133(1):147–157, 2002.

[25] Robert D. Moser, John Kim, and Nagi N. Mansour. Direct numerical simulation of turbulent channel flow up to $Re_\tau = 590$. *Phys. Fluids*, 11(4):943–945, 1999.

[26] Stephen B. Pope. *Turbulent flows*. Cambridge University Press, Cambridge, 2000.

[27] U. Rasthofer and V. Gravemeier. Multifractal subgrid-scale modeling within a variational multiscale method for large-eddy simulation of turbulent flow. *J. Comput. Phys.*, 234:79–107, 2013.

[28] Ursula Rasthofer and Volker Gravemeier. Recent developments in variational multiscale methods for large-eddy simulation of turbulent flow. *Archives of Computational Methods in Engineering*, 25(3):647–690, Jul 2018.

[29] Youcef Saad. A flexible inner-outer preconditioned GMRES algorithm. *SIAM J. Sci. Comput.*, 14(2):461–469, 1993.

[30] Pierre Sagaut. *Large eddy simulation for incompressible flows*. Scientific Computation. Springer-Verlag, Berlin, third edition, 2006. An introduction, Translated from the 1998 French original, With forewords by Marcel Lesieur and Massimo Germano, With a foreword by Charles Meneveau.

[31] J. Smagorinsky. General circulation experiments with the primitive equations. *Mon. Wea. Rev.*, 91:99–164, 1963.

[32] H. A. van der Vorst. Bi-CGSTAB: a fast and smoothly converging variant of Bi-CG for the solution of nonsymmetric linear systems. *SIAM J. Sci. Statist. Comput.*, 13(2):631–644, 1992.

[33] Roel Verstappen. When does eddy viscosity damp subfilter scales sufficiently? *J. Sci. Comput.*, 49(1):94–110, 2011.

[34] Ulrich Wilbrandt, Clemens Bartsch, Naveed Ahmed, Najib Alia, Felix Anker, Laura Blank, Alfonso Caiazzo, Sashikumaar Ganesan, Swetlana Giere, Gunar Matthies, Raviteja Meesala, Abdus Shamim, Jagannath Venkatesan, and Volker John. ParMooN—A modernized program package based on mapped finite elements. *Comput. Math. Appl.*, 74(1):74–88, 2017.